AIAA JOURNAL
Vol. 41, No. 10, October 2003

Effects of Periodic Blowing from Spanwise Slot on a Turbulent Boundary Layer

Kyoungyoun Kim* and Hyung Jin Sung†
Korea Advanced Institute of Science and Technology, Daejeon 305-701, Republic of Korea

Direct numerical simulations were performed to analyze the effects of time-periodical blowing through a spanwise slot on a turbulent boundary layer. The blowing velocity was varied in a cyclic manner from 0 to $2A^+$ ($A^+ = 0.25$, 0.50, and 1.00) at a fixed blowing frequency of $f^+ = 0.017$. The effect of steady blowing (SB) was also examined, and the SB results were compared with those for periodic blowing (PB). PB reduced the skin friction near the slot, although to a slightly lesser extent than SB. PB was found to generate a spanwise vortical structure in the downstream of the slot. This vortex generates a reverse flow near the wall, thereby reducing the wall shear stress. The wall-normal and spanwise turbulence intensities under PB are increased as compared to those under SB, whereas the streamwise turbulent intensity under PB is weaker than that under SB. PB enhances more energy redistribution than SB. The periodic response of the streamwise turbulence intensity to PB is propagated to a lesser extent than that of the other components of the turbulence intensities and the Reynolds shear stress.

I. Introduction

MANY attempts have been made to devise a practical method for controlling wall bounded flows. These include the modification of the wall surface by installing riblets,[1] as well as the use of a compliant wall[2] or a spanwise oscillating wall.[3] Among the approaches considered to date, the use of local suction/blowing deserves more detailed study because it provides an efficient and simple means for locally actuating the wall-bounded flow. Moreover, the strength of the actuation can be controlled with relative ease by local suction/blowing.

Most previous experimental and numerical studies of local suction/blowing have focused on steady actuation. Sano and Hirayama[4] examined the effect of steady blowing or suction through a spanwise slot in a turbulent boundary layer. They found that steady blowing (suction) decreases (increases) skin friction and increases (decreases) turbulent intensity behind the slot. Park and Choi[5] conducted direct numerical simulations to investigate the effects of applying weak steady local blowing or suction. They reported that steady local blowing lifts up the streamwise vortices, thereby reducing the interaction of the vortices with the wall. This leads to a reduction in the skin friction near the slot, combined with an increase in the turbulent intensity and skin friction far downstream from the slot. Krogstad and Kourakine[6] conducted experiments to investigate the effect on a turbulent boundary layer of weak blowing through a porous strip of limited streamwise extent. Kim et al.[7] examined the effect of blowing velocity on the characteristics of the turbulent boundary layer through direct numerical simulations. They conducted simulations at three different values of the blowing velocity under conditions of constant mass flow rate through the slot.

In contrast to the previous studies that considered only steady blowing (SB), Tardu[8] carried out wind-tunnel experiments in which he compared the behavior of a periodically blowing system and a steady-blowing system. He showed that both types of blowing led to a reduction in the skin friction. When the blowing frequency is larger than a critical value ($f_{cr}^+ = 0.008$), the blowing induces a positive wall vorticity layer that subsequently rolls up into a coherent spanwise vortex. Farther downstream, a negative vorticity layer rolls up in its turn. Tardu attempted to explain the response of the flow to periodic blowing in terms of physical arguments based on the vorticity dynamics near the wall. Park et al.[9] performed experiments to probe the effects of periodic blowing and suction through a spanwise slot on a turbulent boundary layer. They showed that increasing the forcing frequency from $f^+ = 0.011$ to 0.044 caused a reduction in the skin friction. The higher forcing frequency induces greater changes in the turbulent structures of boundary layer. Rhee and Sung[10] performed unsteady Reynolds-averaged Navier–Stokes simulations and compared the simulation results with those of the experiments of Park et al.[9] They examined the effect of forcing angle on the skin friction. The flow characteristics downstream of the slot could be mainly related with the spanwise vortical structure caused by the periodic forcing.

In the present study the effect of periodic blowing (PB) on a turbulent boundary layer was investigated through direct numerical simulations of the spatially evolving turbulent boundary layer. In these simulations the Reynolds number based on the momentum thickness at the inlet was $Re_\theta = 300$, which is relatively low compared to the relevant higher-Reynolds-number experimental results. The time-mean blowing velocities were restricted to values smaller than 10% of the free stream velocity ($A^+ = 0.25, 0.50$, and 1.00), and the blowing frequency was fixed at $f^+ = f\nu/u_{\tau,\,\mathrm{in}}^2 = 0.017$, which corresponds to twice the ejection frequency of the inner layer.[8] The objective of the present study was to elucidate the response of a turbulent boundary layer to PB, with particular emphasis on the modulation of the wall shear stress and mean velocities. A spanwise vortical structure was generated by PB, which led to a reduction in the skin friction near the wall. The oscillating components of the turbulent intensities and Reynolds shear stress were analyzed to characterize the unsteady dynamic response of turbulent structure to PB. In addition, a comparison was made between the time-mean velocity, turbulent intensities, and Reynolds shear stress under PB and SB. The budgets of the Reynolds stresses were scrutinized to investigate the energy redistribution caused by PB and SB.

II. Computational Details

As mentioned earlier, a direct numerical simulation of turbulent boundary layer is performed to test the flow. A schematic diagram of the computational domain is displayed in Fig. 1. The domain size is $200\theta_{\mathrm{in}} \times 30\theta_{\mathrm{in}} \times 40\theta_{\mathrm{in}}$ in the streamwise, wall-normal, and spanwise directions, where the corresponding mesh size is $257 \times 65 \times 129$. The mesh is uniform in the streamwise and spanwise directions, but

Received 28 August 2002; revision received 25 February 2003; accepted for publication 12 March 2003.

*Ph.D. Student, Department of Mechanical Engineering, 373-1, Guseong-dong, Yusong-gu.
†Professor, Department of Mechanical Engineering, 373-1, Guseong-dong, Yusong-gu; hjsung@kaist.ac.kr. Member AIAA.

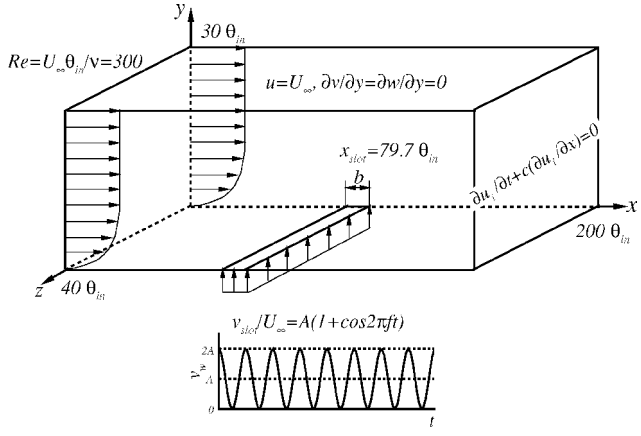

Fig. 1 Schematic diagram of the computational domain.

a hyperbolic tangent stretching is used in the normal direction to cluster points near the wall. The mesh resolutions are $\Delta x^+ \simeq 12.40$, $\Delta y^+_{\min} \simeq 0.17$, $\Delta y^+_{\max} \simeq 23.86$, and $\Delta z^+ \simeq 4.96$, based on the friction velocity at the inlet. Realistic velocity fluctuations at the inlet are obtained using the method of Lund et al.[11] The convective outflow condition $(\partial u_i/\partial t) + c(\partial u_i/\partial x) = 0$ is used at the exit, where c is taken to be the mean exit velocity. A no-slip boundary condition is imposed at the solid wall. At the freestream the conditions $u = U_\infty$ and $\partial v/\partial y = \partial w/\partial y = 0$ are imposed. Periodic boundary conditions are used in the spanwise direction.

The spanwise slot for periodic blowing extends from $x = 75.8\theta_{\text{in}}$ to $x = 82.0\theta_{\text{in}}$, where the location of the inlet is defined as $x = 0$. The slot width is $b^+ \simeq 100$ in wall units. The periodic blowing at the slot is generated by varying the wall-normal velocity according to the equation

$$v_{\text{slot}}/U_\infty = A(1 + \cos 2\pi f t) \tag{1}$$

Thus, the blowing velocity varies periodically between values of 0 and $2A$. As mentioned earlier, the time-mean blowing velocities are restricted to values smaller than 10% of the freestream velocity, that is, $A = 0.0134, 0.0267$, and 0.0534, which correspond to $A^+ = 0.25$, 0.50, and 1.00 in wall units, respectively. Although the forcing amplitudes employed in this study are very small, it has been previously shown that they are sufficient to affect significantly the flow variables and turbulence characteristics in the downstream.[5] The corresponding time-mean flow rates through the slot are $A^+ b^+ = 25$, 50, and 100, respectively. The blowing frequency f is fixed at $f^+ = f\nu/u^2_{\tau,\text{in}} = 0.017$, which corresponds to twice the ejection frequency of the inner layer.[8] The present blowing frequency belongs to the high-frequency excitation region as compared with other forcing cases.[12]

The governing Navier–Stokes and continuity equations are integrated in time by using a fractional step method with an implicit velocity decoupling procedure.[13] A second-order central difference scheme is used in space with a staggered mesh. The Reynolds number based on the momentum thickness at the inlet is $Re_\theta = 300$. The computation time step is $\Delta t U_\infty/\theta_{\text{in}} = 0.3$, which corresponds to $\Delta t^+ \simeq 0.25$ in wall units. The total time over which statistical averages are calculated is $T_{\text{avg}} = 15,000\theta_{\text{in}}/U_\infty$. Each period is divided into 234 phases, and the statistics are obtained by averaging 213 periods.

The imposition of periodic blowing can lead to periodic variations in the global physical quantities of the flow. Hence, it is necessary to represent each flow quantity as a superposition of three components:

$$q(x, y, z, t) = \bar{q}(x, y) + \tilde{q}(x, y, t) + q''(x, y, z, t) \tag{2}$$

where the instantaneous quantity q is decomposed into a time-mean component $\bar{q}$, an oscillating component $\tilde{q}$, and a random fluctuating component q''. The time average is

$$\bar{q}(x, y) = \frac{1}{T_{\text{tot}} L_z} \int_0^{T_{\text{tot}}} \int_0^{L_z} q(x, y, z, t)\, \mathrm{d}z\, \mathrm{d}t \tag{3}$$

where $T_{\text{tot}} = NT$ is the time over which the quantity is averaged and N is the total number of periods. The oscillating component $\tilde{q}$ is obtained from the relation

$$\tilde{q}(x, y, t) = \langle q \rangle(x, y, t) - \bar{q}(x, y) \tag{4}$$

where $\langle q \rangle(x, y, t)$ is the phase average, which is defined as

$$\langle q \rangle(x, y, t) = \frac{1}{NL_z} \sum_{n=1}^{N} \int_0^{L_z} q(x, y, z, t + nT)\, \mathrm{d}z \tag{5}$$

Accordingly, the random fluctuation component q'' is expressed as

$$q''(x, y, z, t) = q(x, y, z, t) - \langle q \rangle(x, y, t) \tag{6}$$

III. Results and Discussion

First, we examine the variations of the mean wall variables along the wall by the present forcing. Figure 2 shows the streamwise distributions of time averages of the skin friction c_f and wall pressure P_w. For both PB and SB c_f decreases rapidly near the slot. Adverse pressure gradients appear upstream and downstream of the slot, whereas a favorable pressure gradient occurs above the slot. The overall characteristics are in good agreement with previous results.[5,7] Previous studies have shown that the application of blowing through a spanwise slot causes the streamwise vorticies to be lifted up, leading to a decrease in the skin friction above the slot. However, this reduction in the skin friction at the slot is accompanied by a slight increase in the skin friction in the downstream caused by the increased turbulence induced by blowing.[5] Inspection of the recovery of the skin friction behind the slot reveals a significant difference between the flow characteristics under PB and SB, although the recovery of the wall pressure collapses well at the same A^+. The difference between the value of c_f for PB and SB increases as A^+ increases (Fig. 2a). Interestingly, the skin friction near the slot is greater for PB than for SB, which suggests that PB reduces the skin friction near the slot to a lesser extent than SB.

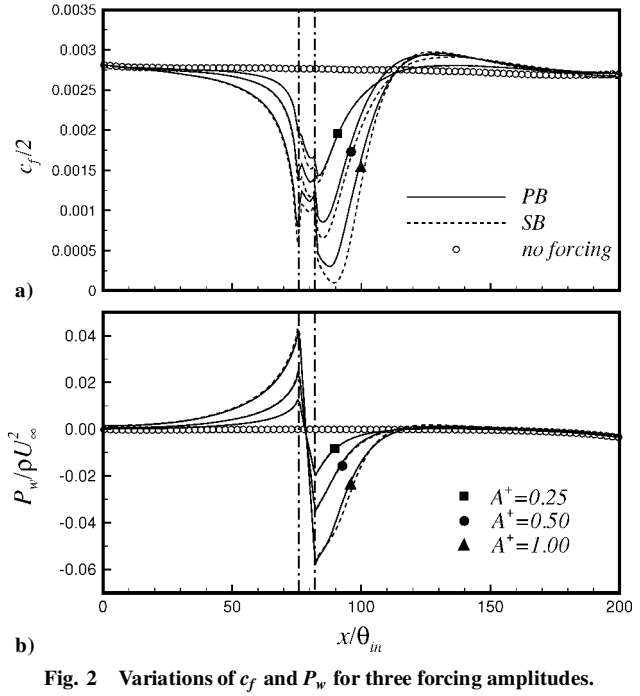

Fig. 2 Variations of c_f and P_w for three forcing amplitudes.

Table 1 Comparison of terms in the time-averaged x momentum at the slot center ($\times 10^{-3}$)

A^+	A^+b^+	$\bar{\sigma}\left(=\frac{\overline{v_{\text{slot}}}b}{U_\infty\theta_{\text{slot}}}\right)$	Blowing type	$\overline{v_{\text{slot}}\frac{\partial\bar{u}}{\partial y}}\Big\vert_w$	$\overline{\tilde{v}_{\text{slot}}\frac{\partial\tilde{u}}{\partial y}}\Big\vert_w$	$-\frac{\partial\bar{p}}{\partial x}\Big\vert_w$	$\frac{1}{Re}\frac{\partial^2\bar{u}}{\partial y^2}\Big\vert_w$
0.25	25	0.068	PB	6.900	−0.997	4.962	0.977
			SB	6.382	——	4.986	1.379
0.50	50	0.136	PB	11.290	−1.703	9.102	0.501
			SB	9.786	——	9.317	0.419
1.00	100	0.272	PB	18.275	−2.438	15.640	0.212
			SB	16.065	——	15.956	0.262

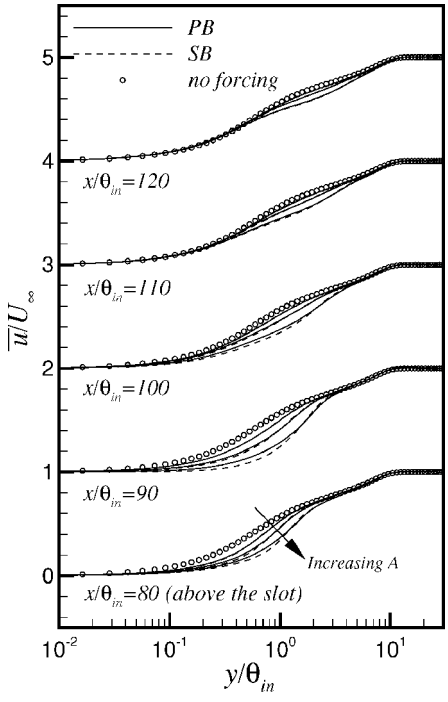

Fig. 3 Time-mean velocity profiles.

To analyze the difference in the skin friction between PB and SB, we examined the time-averaged x momentum at the wall:

$$\overline{v_{\text{slot}}\frac{\partial\bar{u}}{\partial y}}\bigg|_w + \overline{\tilde{v}_{\text{slot}}\frac{\partial\tilde{u}}{\partial y}}\bigg|_w = -\frac{\partial\bar{p}}{\partial x}\bigg|_w + \frac{1}{Re}\frac{\partial^2\bar{u}}{\partial y^2}\bigg|_w \tag{7}$$

The magnitude of each term in Eq. (7) was calculated for three forcing amplitudes at the slot center. As shown in Table 1, the magnitude of $(1/Re)(\partial^2\bar{u}/\partial y^2)|_w$ is relatively small in comparison to the magnitudes of the other terms. This term becomes even smaller as A^+ increases. The magnitude of $-\partial\bar{p}/\partial x|_w$ is almost the same under PB and SB, as can be seen in Fig. 2b. Thus, the magnitude of $\overline{v_{\text{slot}}(\partial\bar{u}/\partial y)}|_w + \overline{\tilde{v}_{\text{slot}}(\partial\tilde{u}/\partial y)}|_w$ under PB is almost equivalent to that under SB. However, because the term $\overline{\tilde{v}_{\text{slot}}(\partial\tilde{u}/\partial y)}|_w$ of SB is zero, it follows that

$$\left(\overline{v_{\text{slot}}\frac{\partial\bar{u}}{\partial y}}\bigg|_w + \overline{\tilde{v}_{\text{slot}}\frac{\partial\tilde{u}}{\partial y}}\bigg|_w\right)_{\text{PB}} \approx \left(\overline{v_{\text{slot}}\frac{\partial\bar{u}}{\partial y}}\bigg|_w\right)_{\text{SB}} \tag{8}$$

As shown in Table 1, the term $\overline{\tilde{v}_{\text{slot}}(\partial\tilde{u}/\partial y)}|_w$ for PB has a negative value. This is because the phase of the blowing velocity is opposite to that of the wall shear stress above the slot. This negative "streaming" gives $[\overline{v_{\text{slot}}}(\partial\bar{u}/\partial y)|_w]_{\text{PB}} > [\overline{v_{\text{slot}}}(\partial\bar{u}/\partial y)|_w]_{\text{SB}}$. Given that the time-mean blowing velocity ($\overline{v_{\text{slot}}}$) under PB is the same as that under SB, we conclude that the skin friction under PB is larger than that under SB.

Figure 3 shows the distributions of the time-mean streamwise velocity in outer coordinates at five streamwise locations ($x/\theta_{\text{in}} = 80$, 90, 100, 110, and 120). A region of retarded flow is observed close to the wall, and the magnitude of this retardation increases with increasing A^+. As the flow moves downstream, the region of retarded flow gradually shifts away from the wall and decays. This is consistent with the finding of Park et al.,[9] where the blowing effect dominates the mean velocity profiles. In the region of $y/\theta_{\text{in}} < 1$ near the slot, the time-mean velocity under PB is slightly greater than that under SB. This is analogous to the difference in skin friction between PB and SB just described. The profiles for both PB and SB collapse at the same value of A^+ except for the region of $y/\theta_{\text{in}} < 1$ near the slot. The time-mean streamwise velocity profiles are seen to be insensitive to the present blowings.[8]

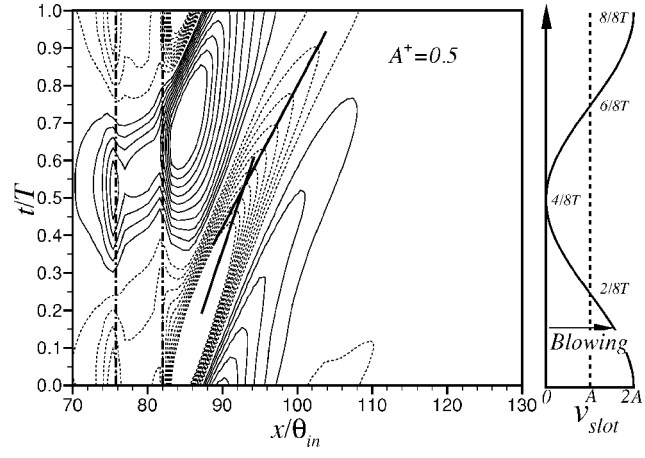

Fig. 4 Spatio-temporal evolution of the relative modulations of wall shear stress ($A^+ = 0.5$). The contour levels range from −1 to 1 by increments of 0.1.

Figure 4 shows the spatio-temporal evolutions of the relative modulation of wall shear stress ($\tilde{\tau}_w/\overline{\tau_w}$) during one period of blowing. The relative modulation indicates the unsteady response of the wall shear stress ($\tilde{\tau}_w = \langle\tau_w\rangle - \overline{\tau_w}$) to the imposed periodic blowing. As time proceeds, $\tilde{\tau}_w/\overline{\tau_w}$ changes considerably close to the slot. The phase of the blowing velocity v_{slot} is opposite to that of $\tilde{\tau}_w$ above the slot. A region of lower wall shear stress is observed near the slot, and it decays in the downstream region ($x/\theta_{\text{in}} > 110$). The convection velocity is detected by tracing the lower wall shear stress region, which is denoted by a thick solid line in Fig. 4. The convection velocity increases slightly on moving downstream. This is consistent with the results of Rhee and Sung,[10] who found that the temporal variation of the local minimum of skin friction corresponds to the trajectory of the large-scale vortex generated by the local forcing.

Figure 5 shows contour plots of the oscillating components of the spanwise vorticity ($\tilde{\omega}_z$) along with the vectors of the oscillating components of the velocity ($\tilde{u},\tilde{v}$). Eight snapshots taken at intervals of $T/8$ are shown, where T is the blowing period. As in Fig. 4, the maximum blowing is imparted at $t = 0$ and the minimum at $t = 4T/8$. The velocity vectors in Fig. 5 clearly show the generation of a strong spanwise vortical structure caused by the periodic blowing, and this vortex convects downstream over time. During the phase of maximum blowing, the incoming freestream is temporarily blocked by the strong upward motion. The pressure in the close

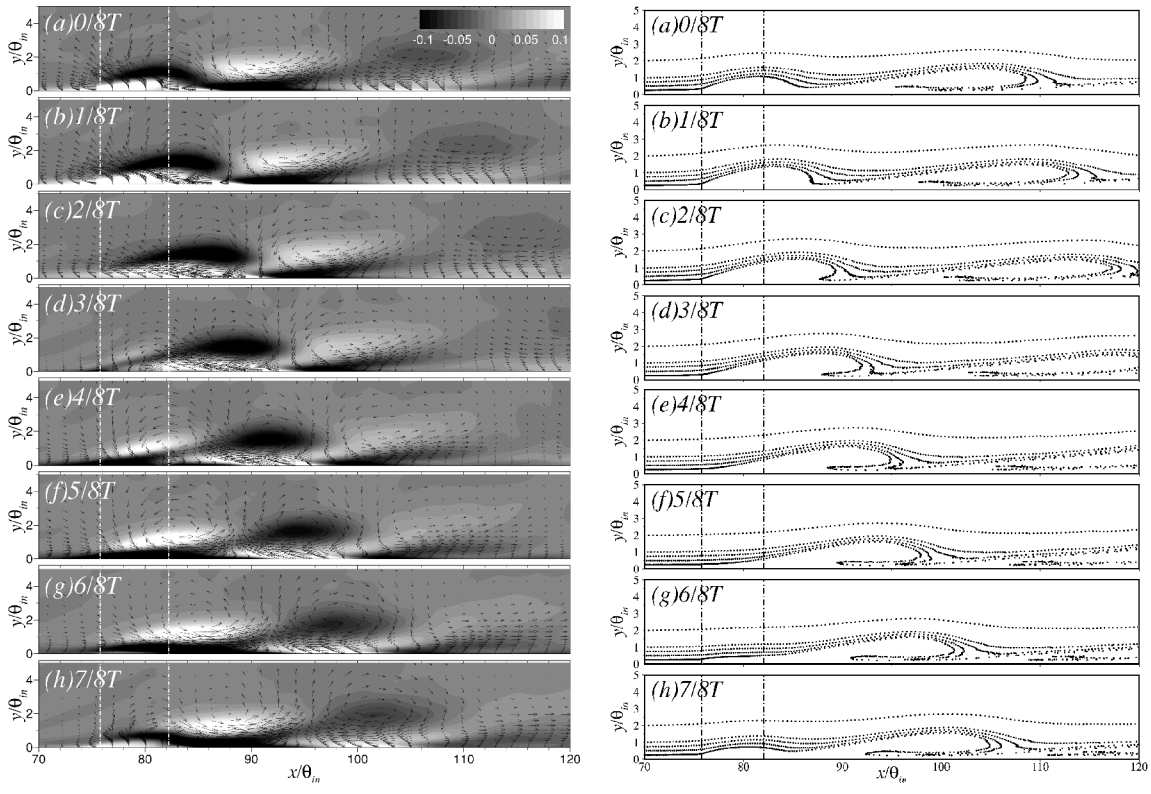

Fig. 5 Contour plots of the oscillating components of spanwise vorticity with the oscillating components of velocity vectors (left) and streaklines (right) for $A^+ = 0.5$.

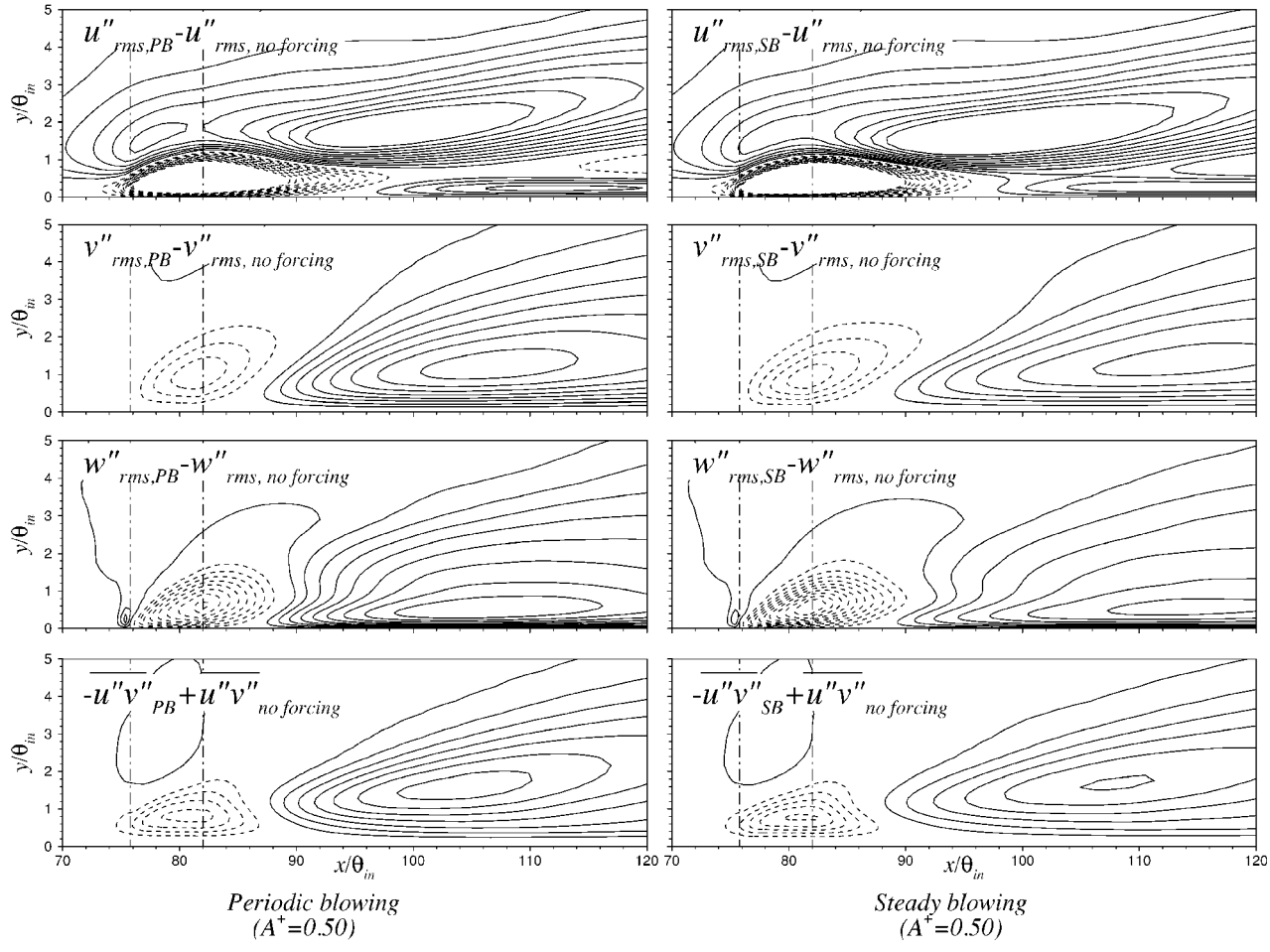

Fig. 6 Contours of the differences of the time-averaged rms velocity fluctuations and Reynolds shear stress. Contour levels are from $-0.02\,U_\infty$ to $0.02\,U_\infty$ by increments of 0.002 for the velocity fluctuations and from $-0.002\,U_\infty^2$ to $0.002\,U_\infty^2$ by increments of 0.0002 for the Reynolds shear stress.

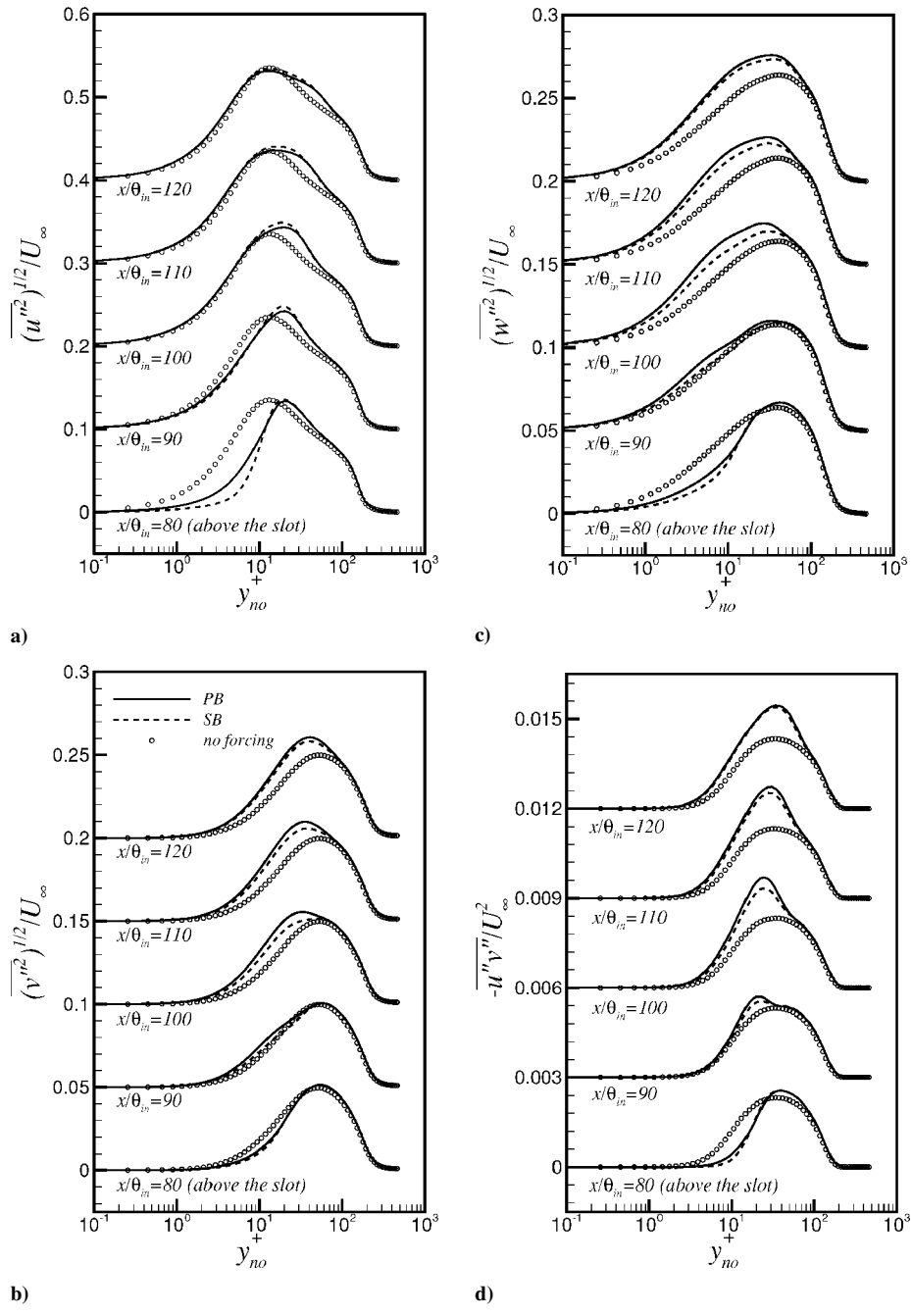

Fig. 7 Variations of time-averaged turbulent intensities and Reynolds shear stress for $A^+ = 0.5$: a) $u''_{\rm rms}$, b) $v''_{\rm rms}$, c) $w''_{\rm rms}$, and d) $-\overline{u''v''}$.

downstream vicinity of the slot abruptly decreases, leading to the formation of a reverse flow region. At the beginning of the minimum blowing phase, this reverse flow region becomes larger such that it engulfs the preinjected fluid and a vortical structure is created. This vortex generates a reverse flow near the wall, thereby reducing the wall-region velocity. As the flow moves downstream, the large-scale vortical structure gradually shifts away from the wall and increases in size. To more clearly observe the vortex formation process in the presence of periodic blowing, streaklines are plotted in Fig. 5 over one blowing period. The vortex with negative ω_z induces a negative streamwise velocity in the vicinity of the wall.[14] This leads to the reduction of skin friction, which is closely related to the convection velocity of the local minimum of $\widetilde{\tau_w}/\overline{\tau_w}$ in the downstream in Fig. 4.

Imposition of a local forcing (PB or SB) leads to a decrease in the velocity fluctuations and Reynolds shear stress near the slot. These quantities decrease because the fluid is lifted away from the wall by the blowing. However, the velocity fluctuations and Reynolds shear stress are significantly enhanced downstream of the slot. Figure 6 shows contours of the difference between the rms velocity fluctuations under the present forcings (PB and SB) and the values under the "no-forcing" condition. This figure also shows the corresponding contours for the Reynolds shear stress. The global features of $v''_{\rm rms}$, $w''_{\rm rms}$, and $-\overline{u''v''}$ are quite similar, but $u''_{\rm rms}$ shows different behavior. Under both PB and SB, the maximum change of $u''_{\rm rms}$ is located closer to the slot than the maximum changes of $v''_{\rm rms}$, $w''_{\rm rms}$, and $-\overline{u''v''}$. Note that the maximum changes of $v''_{\rm rms}$, $w''_{\rm rms}$, and $-\overline{u''v''}$ for PB are located closer to the slot than those for SB. This indicates that the velocity fluctuations $v''_{\rm rms}$ and $w''_{\rm rms}$ and the Reynolds shear stress ($-\overline{u''v''}$) respond more quickly to PB than to SB.

Profiles of the rms velocity fluctuations ($u''_{\rm rms}$, $v''_{\rm rms}$, and $w''_{\rm rms}$) and Reynolds shear stress ($-\overline{u''v''}$) are shown in Fig. 7. As just mentioned, the velocity fluctuations and Reynolds shear stress are attenuated near the slot ($x/\theta_{\rm in} = 80$) but are enhanced downstream of the slot ($x/\theta_{\rm in} \geq 100$) for both PB and SB. The maximum change of $u''_{\rm rms}$ is observed at $x/\theta_{\rm in} = 100$, whereas the maximum changes of $v''_{\rm rms}$, $w''_{\rm rms}$, and $-\overline{u''v''}$ are located in the far downstream ($x/\theta_{\rm in} \geq 110$).

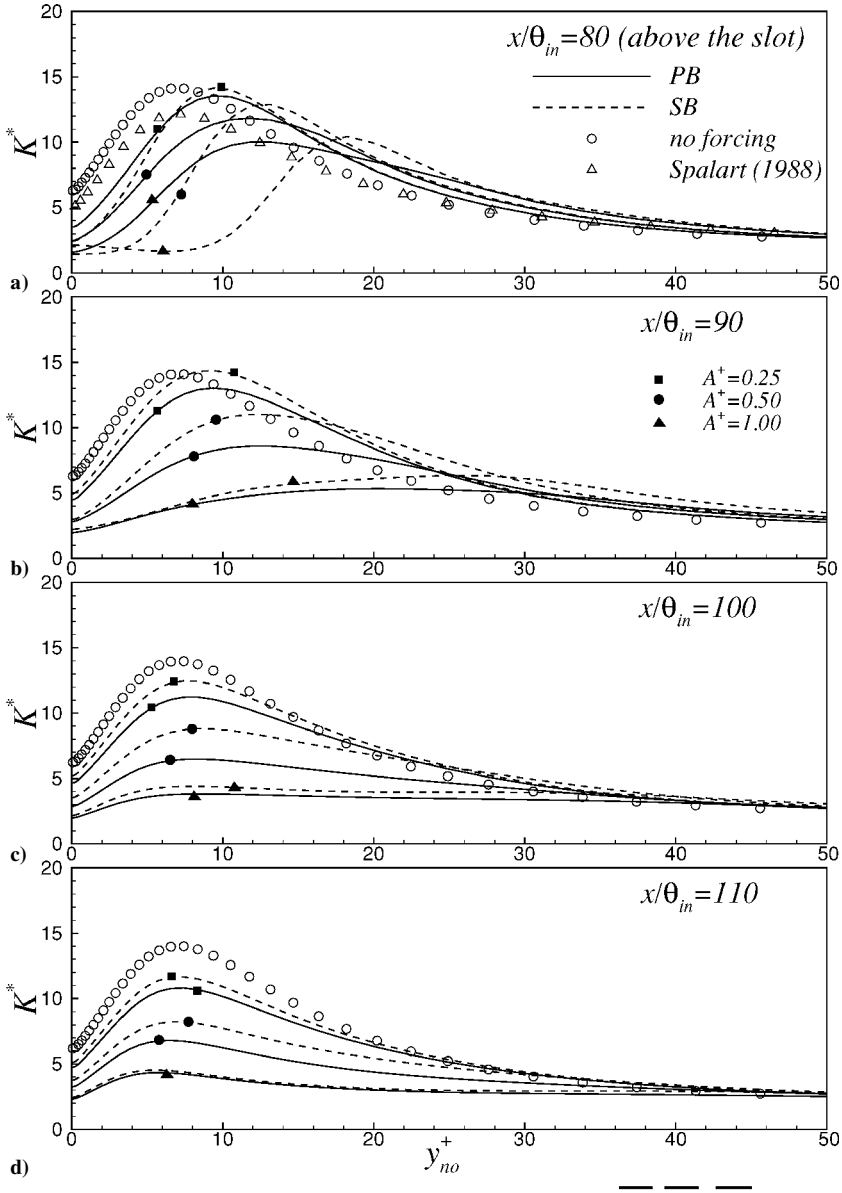

Fig. 8 Variations of the energy partition parameter $K^* = 2\overline{u''^2}/(\overline{v''^2} + \overline{w''^2})$.

The increases in $v''_{\rm rms}$ and $w''_{\rm rms}$ for PB are larger than those for SB, whereas the increase in $u''_{\rm rms}$ for PB is slightly smaller than that for SB. This suggests that PB enhances the energy redistribution in the streamwise downstream more strongly than SB does.

To examine the energy redistribution altered by the local forcings, the energy partition parameter $K^* = 2u''^2/(v''^2 + w''^2)$ is employed.[15] This parameter is a measure of the relative contribution to the turbulent kinetic energy of the streamwise turbulence intensity and the intensities normal to the mean flow.[16] As shown in Fig. 8,[17] K^* significantly decreases near the wall for both PB and SB in comparison with the no-forcing case. Above the slot ($x/\theta_{\rm in} = 80$) the values of K^* for SB are smaller than those for PB in the vicinity of the wall ($y^+ \leq 10$). However, the values of K^* for PB are smaller than those for SB in the downstream ($x/\theta_{\rm in} \geq 90$). The amount of energy transfer from the streamwise velocity component to the other two velocity components under PB is generally larger than that under SB.

The budgets of $\overline{u''^2}$, $\overline{v''^2}$, and $\overline{w''^2}$ are analyzed to examine the energy redistribution just mentioned. The transport equation for the time-averaged Reynolds-stress components is expressed as

$$\frac{\partial \overline{u''_i u''_j}}{\partial t} = 0 = \underbrace{-\overline{\left(\langle u''_i u''_k \rangle \frac{\partial \langle u_j \rangle}{\partial x_k} + \langle u''_j u''_k \rangle \frac{\partial \langle u_i \rangle}{\partial x_k} \right)}}_{\text{production}} \underbrace{-\overline{\langle u_k \rangle \frac{\partial \langle u''_i u''_j \rangle}{\partial x_k}}}_{\text{convection}}$$

$$\underbrace{-\frac{\partial \overline{u''_i u''_j u''_k}}{\partial x_k}}_{\text{turbulent transport}} \underbrace{-\frac{2}{Re}\overline{\frac{\partial u''_i}{\partial x_k}\frac{\partial u''_j}{\partial x_k}}}_{\text{dissipation}} \underbrace{+\frac{1}{Re}\frac{\partial^2 \overline{u''_i u''_j}}{\partial x_k{}^2}}_{\text{viscous diffusion}}$$

$$\underbrace{+\overline{p''\left(\frac{\partial u''_i}{\partial x_j} + \frac{\partial u''_j}{\partial x_i}\right)}}_{\text{pressure-strain}} \underbrace{-\frac{\partial \overline{p''(u''_i \delta_{jk} + u''_j \delta_{ik})}}{\partial x_k}}_{\text{pressure transport}} \tag{9}$$

The budgets of $\overline{u''^2}$, $\overline{v''^2}$, and $\overline{w''^2}$ for PB and SB are shown in Fig. 9. The thick and thin lines denote the profiles of PB and SB, respectively. The budgets are significantly disturbed by the forcings near the slot; however, by $x/\theta_{\rm in} = 140$ they have mostly recovered to the values observed under the no-forcing condition. In the budget of u''^2 shown in Fig. 9a for both PB and SB, the production term is in balance with the dissipation and pressure-strain terms away from the wall, whereas the diffusion and dissipation terms are dominant close to the wall. Above the slot the viscous diffusion and turbulent transport terms for PB are much smaller than those for SB. In the near downstream of the slot ($x/\theta_{\rm in} = 90$ and 100), the behavior of u''^2 is very similar for PB and SB, with the exception of the pressure-strain term. At these locations ($x/\theta_{\rm in} = 90$ and 100) the

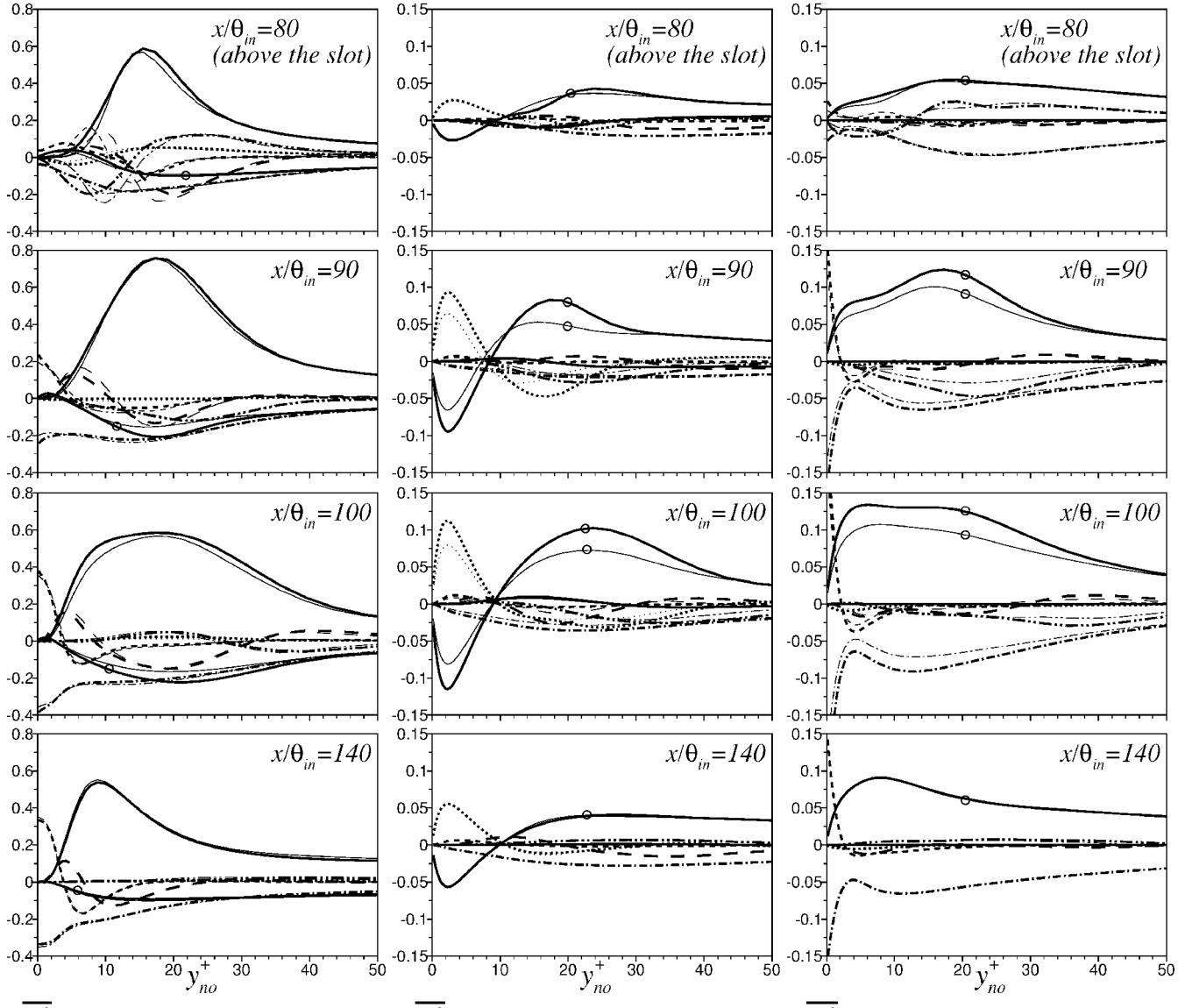

a) $\overline{u''^2}$ budget b) $\overline{v''^2}$ budget c) $\overline{w''^2}$ budget

Fig. 9 Terms in the budget of $\overline{u''^2}$, $\overline{v''^2}$, and $\overline{w''^2}$, nondimensionalized by $u^4_{\tau,\text{no forcing}}/\nu$ ($A^+ = 0.5$): ——, production; – – –, dissipation; - - - -, viscous diffusion; – - – -, convection; – – –, turbulent transport; · · · ·, pressure transport; and ○, pressure strain.

magnitude of the pressure-strain term is greater for PB than for SB. The budgets of $\overline{v''^2}$ and $\overline{w''^2}$ are shown in Figs. 9b and 9c, respectively. Note that the production terms in the $\overline{v''^2}$ and $\overline{w''^2}$ budgets are negligible, and the pressure-strain term is dominant except in the vicinity of the wall. Similar to the $\overline{u''^2}$ budget, the pressure-strain term for PB is larger than that for SB in the near downstream of the slot.

It is known that the pressure-strain term $\phi_{ij} = \overline{p''(\partial u_i''/\partial x_j + \partial u_j''/\partial x_i)}$ plays a dominant role in the energy redistribution among the components.[18] The negative sign of ϕ_{kk} (no summation) indicates a loss of energy from $\overline{u_k''^2}$ or a transfer of energy from this component to other components, whereas the positive sign of ϕ_{kk} (no summation) denotes an energy gain. In the downstream ($x/\theta_{\text{in}} > 90$) the magnitudes of ϕ_{kk} (no summation) for PB are larger than those for SB. This indicates that more energy is redistributed under PB than under SB, which is in agreement with the behavior of the energy partition parameter K^* shown in Fig. 8.

To examine the unsteady dynamic response of the turbulence structure to the PB imposed in the present study, we consider the oscillating components of the turbulent intensities (u''^2, v''^2, and w''^2) and the Reynolds shear stress ($-u''v''$) over one period of blowing. A sequence of eight snapshots showing the evolution of the oscillating components is plotted in Fig. 10. The vector plots of the oscillating velocity components are superimposed to gain a better understanding of the flow evolution. In the contour plots of u''^2 (Fig. 10a), the unsteady response of u''^2 to the PB is significant above the slot, and it gradually decays downstream. The oscillating component above the slot is negative during the blowing phases $0/8T \sim 2/8T$ and is positive during the phases $4/8T \sim 6/8T$. Closer inspection of the u''^2 contours reveals the generation of a positive weak oscillating component downstream of the slot ($t = 5/8T$). Examination of the streaklines in Fig. 5 further discloses that this positive oscillating component is created at the bottom left of the spanwise vortical structure. The positive oscillating component of u''^2 is generated as a result of the enhancement of the production term of $\langle u''^2 \rangle$ by the strain rates induced by the spanwise vortical structure, that is, $\hat{P}_{11} = -2(\langle u''^2 \rangle \partial\langle u \rangle/\partial x + \langle u''v'' \rangle \partial\langle u \rangle/\partial y)$ is activated by the strain rates ($\partial\tilde{u}/\partial x < 0$, $\partial\tilde{u}/\partial y > 0$).

The evolution of v''^2 (Fig. 10b), similar to u''^2, shows that the oscillating component is negative above the slot during the blowing phases $0/8T \sim 2/8T$ and is positive during the phases $4/8T \sim 6/8T$. However, v''^2 gradually strengthens in the downstream, whereas u''^2 is confined to near the slot. Downstream of the slot, a positive oscillating component is created at the right bottom of the spanwise

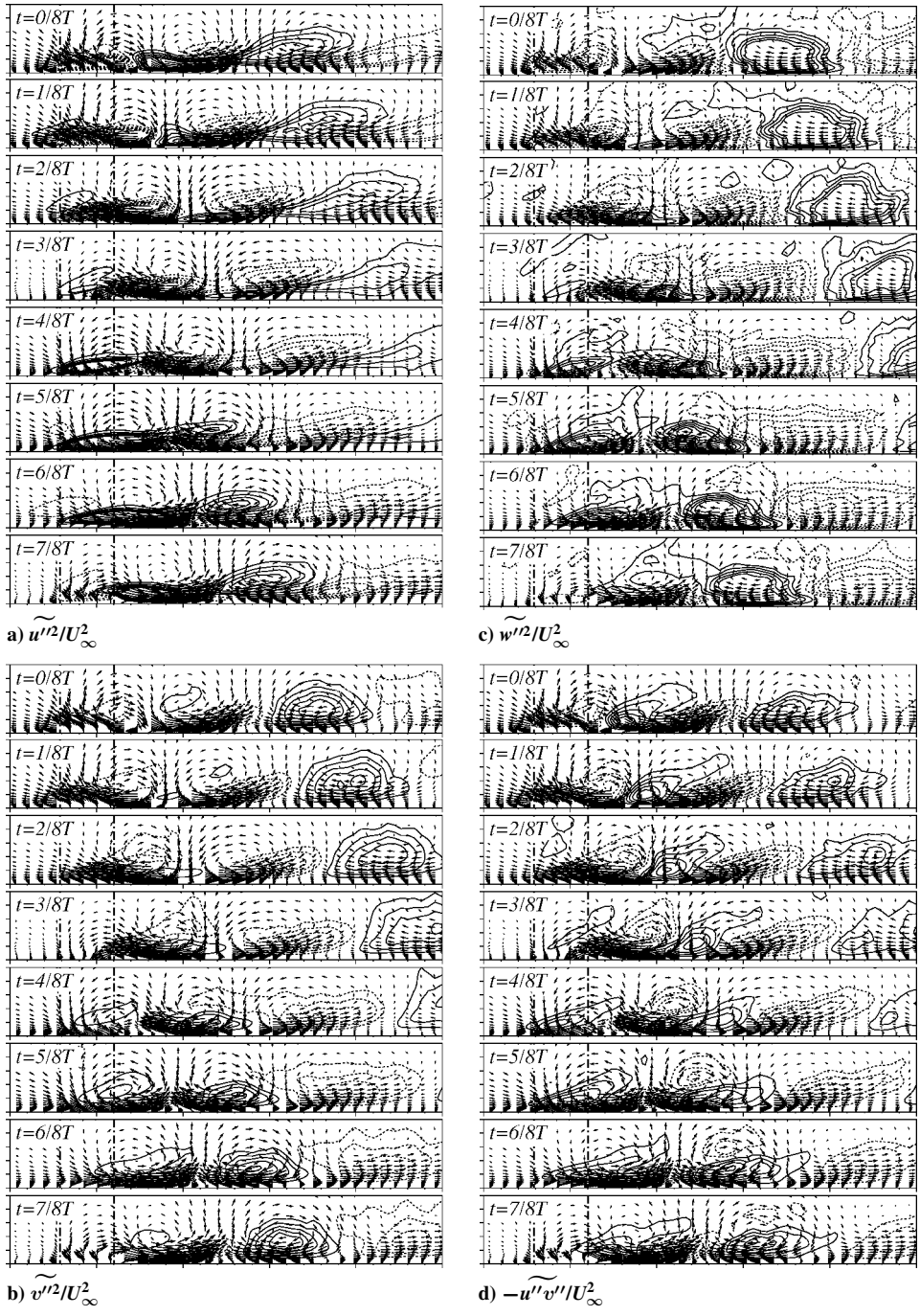

Fig. 10 Contours of the oscillating component of turbulent intensities and Reynolds shear stress ($A^+ = 0.5$). Contour levels are from -0.004 to 0.004 by increments of 0.0008 for $\widetilde{u''^2}/U_\infty^2$ and from -0.001 to 0.001 by increments of 0.0002 for $\widetilde{v''^2}/U_\infty^2$, $\widetilde{w''^2}/U_\infty^2$, and $-\widetilde{u''v''}/U_\infty^2$. The plot domain is $70 \le x/\theta_{in} \le 120$ and $0 \le y/\theta_{in} \le 5$.

vortical structure in the phase $t = 2/8T$. The production term of $\langle v''^2 \rangle$ becomes significant because of the strain rates of the spanwise vortical structure, whereas the production in the v''^2 budget is negligible. The spanwise vortical structure induces a "downwash," which leads to $\partial \tilde{v}/\partial y < 0$ at the right bottom of the vortical structure. Because this oscillating component of the strain rates enhances the production term $\hat{P}_{22} = -2(\langle v''^2 \rangle \partial \langle v \rangle / \partial y + \langle u''v'' \rangle \partial \langle v \rangle / \partial x)$, the positive oscillating component of v''^2 is generated. The global behavior of $\widetilde{w''^2}$ is very similar to that of $\widetilde{v''^2}$ (Fig. 10c). This indicates that the unsteady effect of PB on u''^2 is confined to near the slot, whereas the unsteady effect of PB on v''^2 and w''^2 is propagated further downstream. In the contour plots of $-u''v''$ (Fig. 10d), a negative oscillating component is observed above the slot at the maximum blowing ($t = 0/8T$); this negative oscillating component is engulfed in the spanwise vortical structure and then convects downstream. In contrast, a positive oscillating component is observed above the slot at the minimum blowing ($t = 4/8T$). The positive oscillating component is not engulfed into the region of $\widetilde{\omega_z} > 0$. This is because the positive modulation of spanwise vorticity ($\widetilde{\omega_z} > 0$) is not a real vortical structure as shown in Fig. 5.

IV. Conclusions

A detailed numerical analysis was performed to delineate the effects of periodic blowing through a spanwise slot on a turbulent boundary layer. Statistical descriptions of flow quantities were obtained by performing direct numerical simulations of the spatially evolving turbulent boundary layer at $Re_\theta = 300$ for three blowing amplitudes ($A^+ = 0.25$, 0.50, and 1.00) with the same blowing

frequency ($f^+ = 0.017$). The simulation results show that periodic blowing reduces the skin friction close to the slot and increases the turbulent intensities and Reynolds shear stress in the downstream. Inspection of the time-dependent contour plots of the spanwise vorticity and streaklines revealed the formation of a spanwise vortical structure. This structure was closely related to the region of lower wall shear stress downstream of the slot. Investigation of the oscillating components of the turbulent intensities and Reynolds shear stress showed that the unsteady response of the streamwise turbulent intensity (u''^2) to PB is propagated to a lesser extent than the unsteady responses of the intensities normal to the mean flow and the Reynolds shear stress (v''^2, w''^2, and $-u''v''$). A systematic comparison was made between the behavior of the time-mean velocity, turbulent intensities, and Reynolds shear stress under PB and SB. Near the slot the skin friction of PB is larger than that of SB because of the negative streaming induced by PB. The cross-stream turbulent intensity and Reynolds shear stress are enhanced to a greater extent for PB than for SB. In addition, the wall-normal and spanwise velocity fluctuations as well as the Reynolds shear stress respond more quickly to PB than to SB. Examination of the energy partition parameter showed that the amount of energy transfer from the streamwise velocity component to the other two velocity components was larger under PB than under SB. This was confirmed by evaluating the pressure-stain correlation tensor in the Reynolds-stress budget analysis.

Acknowledgment

This research was supported by a grant from the National Research Laboratory of the Ministry of Science and Technology, Republic of Korea.

References

[1]Choi, H., Moin, P., and Kim, J., "Direct Numerical Simulation of Turbulent Flow over Riblets," *Journal of Fluid Mechanics*, Vol. 255, 1993, pp. 503–539.

[2]Choi, K. S., Yang, X., Clayton, B. R., Glover, E. J., Atlar, M., Semenov, B. N., and Kulik, V. M., "Turbulent Drag Reduction Using Compliant Surfaces," *Proceedings of the Royal Society of London Series A*, Vol. 453, 1997, pp. 2229–2240.

[3]Choi, J.-I., Xu, C.-X., and Sung, H. J., "Drag Reduction by Spanwise Wall Oscillations in Wall-Bounded Turbulent Flows," *AIAA Journal*, Vol. 40, No. 5, 2002, pp. 842–850.

[4]Sano, M., and Hirayama, N., "Turbulent Boundary Layers with Injection and Suction Through a Slit. First Report: Mean and Turbulence Characteristics," *Bulletin of the Japan Society of Mechanical Engineers*, Vol. 28, No. 239, 1985, pp. 807–814.

[5]Park, J., and Choi, H., "Effects of Uniform Blowing or Suction from a Spanwise Slot on a Turbulent Boundary Layer Flow," *Physics of Fluids*, Vol. 11, No. 10, 1999, pp. 3095–3105.

[6]Krogstad, P. Å., and Kourakine, A., "Some Effects of Localized Injection on the Turbluence Structure in a Boundary Layer," *Physics of Fluids*, Vol. 12, No. 11, 2000, pp. 2990–2999.

[7]Kim, K., Sung, H. J., and Chung, M. K., "Assessment of Local Blowing and Suction in a Turbulent Boundary Layer," *AIAA Journal*, Vol. 40, No. 1, 2002, pp. 175–177.

[8]Tardu, S. F., "Active Control for Near-Wall Turbulence by Local Oscillating Blowing," *Journal of Fluid Mechanics*, Vol. 439, 2001, pp. 217–253.

[9]Park, S.-H., Lee, I., and Sung, H. J., "Effect of Local Forcing from a Spanwise Slot on a Turbulent Boundary Layer," *Experiments in Fluids*, Vol. 31, 2000, pp. 384–393.

[10]Rhee, G. H., and Sung, H. J., "Numerical Prediction of Locally-Forced Turbulent Boundary Layer," *International Journal of Heat and Fluid Flow*, Vol. 22, No. 6, 2001, pp. 624–632.

[11]Lund, T. S., Wu, X., and Squires, K. D., "Generation of Turbulent Inflow Data for Spatially-Developing Boundary Layer Simulation," *Journal of Computational Physics*, Vol. 140, 1998, pp. 233–258.

[12]Scotti, A., and Piomelli, U., "Numerical Simulation of Pulsating Turbulent Channel Flow," *Physics of Fluids*, Vol. 13, No. 5, 2001, pp. 1367–1384.

[13]Kim, K., Baek, S.-J., and Sung, H. J., "An Implicit Velocity Decoupling Procedure for the Incompressible Navier–Stokes Equations," *International Journal for Numerical Method in Fluids*, Vol. 38, No. 2, 2002, pp. 125–138.

[14]Rajagopalan, S., and Antonia, R. A., "Structure of the Velocity Field Associated with the Spanwise Vorticity in the Wall Region of a Turbulent Boundary Layer," *Physics of Fluids*, Vol. 5, No. 10, 1993, pp. 2502–2510.

[15]Lee, M. J., Kim, J., and Moin, P., "Structure of Turbulence at High Shear Rate," *Journal of Fluid Mechanics*, Vol. 216, 1990, pp. 561–583.

[16]Neves, J. C., Moin, P., and Moser, R. D., "Effects of Convex Transverse Curvature on Wall-Bounded Turbulence. Part 1: Time Velocity and Vorticity," *Journal of Fluid Mechanics*, Vol. 272, 1994, pp. 349–381.

[17]Spalart, P. R., "Direct Simulation of a Turbulent Boundary Layer up to $Re_\theta = 1410$," *Journal of Fluid Mechanics*, Vol. 187, 1988, pp. 61–98.

[18]Mansour, N. N., Kim, J., and Moin, P., "Reynolds-Stress and Dissipation-Rate Budgets in a Turbulent Channel Flow," *Journal of Fluid Mechanics*, Vol. 194, 1988, pp. 15–44.

R. M. C. So
Associate Editor